photocorrosion. Even for small Pt coverages (10-20%) most of the holes transit towards solution via the very Pt grains, provided that their density $N_o > 10^{12}$ cm^{-2}, because of surface diffusion. No marked improvement of the transfer kinetics is detected. Such modified electrodes prove to be of interest because their photovoltaic properties are better than those of a naked electrode or those of a solid Schottky barrier.

Acknowledgments

The authors are pleased to thank Dr. Cachet and J. N. Chazalviel for valuable discussions, and F. Pillier and P. Delichere for the TEM observations and the RBS measurements, respectively. This work is supported by both GRECO 130061 and 86.

Manuscript submitted Dec. 21, 1987; revised manuscript received Aug. 15, 1988. This was Paper 856 presented at the Honolulu, HI, Meeting of the Society, Oct. 18-23, 1987.

Centre National de la Recherche Scientifique assisted in meeting the publication costs of this article.

REFERENCES

1. Y. Nakato, T. Ohnishi, and H. Tsubomura, *Chem. Lett.*, 883 (1975).
2. Y. Nakato, K. Abe, and H. Tsumobura, *Ber. Bunsenges. Phys. Chem.*, **80,** 1002 (1976).
3. S. Menezes, A. Heller, and B. Miller, *This Journal,* **127,** 1268 (1980).
4. K. W. Frese, Jr., M. J. Madou, and S. R. Morrison, *ibid.*, **128,** 1939 (1981).
5. J. D. Porter, A. Heller, and D. E. Aspnes, *Nature,* **313,** 664 (1985).
6. Y. Nakato, K. Ueda, and H. Tsubomura, *J. Phys. Chem.*, **90,** 5495 (1980).
7. A. Heller, E. Aharon-Shalom, W. A. Bonner, and B. Miller, *J. Am. Chem. Soc.*, **104,** 6942 (1982).
8. Y. Nakato, H. Yano, S. Nishiura, K. Ueda, and H. Tsubomura, *J. Electroanal. Chem.*, **228,** 97 (1987).
9. Y. Nakato and H. Tsubomura, *J. Photochem.*, **29,** 257 (1985).
10. P. Allongue, E. Souteyrand, L. Allemand, and H. Cachet, Abstract 856, p. 1215, The Electrochemical Society Extended Abstracts, Vol. 87-7, Honolulu, HI, Oct. 18-23, 1987.
11. P. Allongue and E. Souteyrand, *J. Vac. Sci. Technol.*, **B5**(6), 1644 (1987).
12. P. Allongue and H. Cachet, *Solid State Comm.*, **55,** 49 (1985).
13. P. Allongue and H. Cachet, *Ber. Bunsenges. Phys. Chem.*, **91,** 386 (1987).
14. a, P. Allongue and H. Cachet, *ibid.*, **92,** 566 (1988); b, P. Allongue, *ibid.*, In press.
15. F. Abel, G. Amsel, M. Bruneaux, C. Cohen, and A. L'Hoir, *Phys. Rev. B.*, **12,** 4617 (1975).
16. P. Allongue and E. Souteyrand, To be published.
17. J. E. A. M. Van den Meerakker, *Electrochim. Acta,* **30,** 1063 (1985).
18. P. Allongue, H. Cachet, P. Clechet, M. Froment, J. R. Martin, and E. Verney, *This Journal,* **134,** 620 (1987).
19. P. Allongue and H. Cachet, *Electrochim. Acta,* **33,** 693 (1988).
20. J. Reichman *Appl. Phys. Lett.*, **36,** 574 (1980).
21. S. Doniach, K. K. Chin, I. Lindau, and W. E. Spicer, *Phys. Rev. Lett.*, **58,** 591 (1987).
22. E. H. Roderick, in "Metal Semiconductor Contacts" Clarendon Press, Oxford (1980).
23. S. M. Sze, Physics of Semiconductor Devices," John Wiley & Sons, Inc., New York (1969).
24. F. Decker, B. Pettinger, and H. Gerischer, *This Journal,* **130,** 1335 (1983).
25. Y. Nakato, K. Ueda, H. Yano, and H. Tsubomura, *J. Phys. Chem.*, **92,** 2316 (1988).

Semiconductor Electrodes, 62. Photoluminescence and Electroluminescence from Manganese-Doped ZnS and CVD ZnS Electrodes

Jiangbo Ouyang, Fu-Ren F. Fan, and Allen J. Bard*

Department of Chemistry, The University of Texas, Austin, Texas 78712

ABSTRACT

The photoluminescence (PL) and electroluminescence (EL) from single-crystal Mn-doped ZnS (ZnS:Mn) centered at 580 nm was investigated. The PL was quenched by surface modification with I_2- treated poly(vinylferrocene). The effect of *p*H and temperature on the EL of ZnS:Mn in aqueous and butyronitrile solutions upon reduction of peroxydisulfate ion was also studied. EL of polycrystalline chemical vapor deposited (CVD) ZnS doped with Al, Cu-Al, and Mn was also observed with peaks at 430, 475, and 565 nm, respectively. In all cases, the EL efficiency was about 0.2%-0.3%.

Luminescence studies of semiconductors immersed in liquids provide a useful probe of surface recombination and other surface processes. For example, electroluminescence (EL) at chalcogenide semiconductor electrodes [*e.g.*, CdS, CdSe, and CdTe (1)] has been the subject of a number of studies. Single-crystal ZnS has also been used in EL studies (2). ZnS is a wide bandgap (3.66 eV) II-VI compound semiconductor and an excellent EL material (3). Previous experimental results (1-3) suggested that it would be of interest to examine the EL of ZnS as a probe of the energetics at the ZnS/electrolyte interface and for possible application to display devices (2a).

Mn-doped (ZnS:Mn) is an efficient luminescent inorganic solid (4). Manganese is an efficient luminescence activator in a number of host lattices, *e.g.*, silicates, sulfides, and fluorides of zinc or cadmium (5), and plays an important role in the electroluminescence of group II-VI compounds. Although much work has been done over the last few decades to understand the photoluminescence (PL) and EL mechanisms in Mn luminescence centers and in group II-VI compounds doped with Mn, no work has been reported on the EL of ZnS:Mn in liquid junction cells. This paper concerns the EL at ZnS:Mn electrodes in aqueous solutions where emission typical of manganese was observed at 580 nm. A general strategy for designing optically coupled sensors with chemical specificity has attracted much attention (7), and photoluminescence from surface-modified ZnS:Mn has been studied for this purpose. We also studied EL of ZnS:Mn in a butyronitrile solution containing persulfate at different temperatures and have shown that the spectral distribution of EL is independent of temperature. The EL efficiency of ZnS:Mn in persulfate solution was found to be 0.3%. Finally, commercially available single-crystal ZnS is expensive, because it is difficult to grow high-quality, large-area, single crystals of ZnS. Large-area polycrystalline materials can be grown by chemical vapor deposition (CVD). Experi-

* Electrochemical Society Active Member.

ments were performed to test the utility of CVD ZnS electrodes for EL.

Experimental

Single-crystal ZnS:Mn (1% Mn, 0.01% Al, and Zn-treated) was generously donated by Professor J. McCaldin (California Institute of Technology, Los Angeles, California). The CVD ZnS material was purchased from CVD Incorporated (Woburn, Massachusetts). As received, the material was transparent and yellowish and showed a high resistivity ($\geq$20 MΩ-cm). The specimen was cut into slices 0.5 × 0.5 × 0.1 cm. These slices were washed in acetone and ethanol in an ultrasonic bath. To decrease the resistivity, the slices were heated at 900°C for 36h with mixtures of different metals: Zn:Al (1:1) metals (both 99.9999%, from Alfa Products, Danvers, Massachusetts) for Al-doped ZnS; with Zn:Al:Cu (1:1:1) for Cu, Al-doped ZnS; and with Zn:Al:Mn (1:1:1) for Mn, Al-doped ZnS (99.999% Cu from AESAR, Seabrook, New Hampshire). All the slices with metals were sealed under vacuum ($\leq 10^{-4}$ torr) in a quartz tube at room temperature. After this treatment, the doped ZnS slices were heated again with Zn powder at 900°C for 4h. This treatment lowered the resistivity of the material to 100-1000 Ω-cm. Ohmic contact was made by In:Ga (1:3) alloy according to the method of Kaufman and Dowbor (8). The electrode was mounted as previously described (9). The electrode was etched in a $K_2Cr_2O_7$-H_2SO_4 (cleaning) solution at 70°C for 5 min. In experiments where the Mn-ZnS surface was modified with a polymer layer, a CH_2Cl_2 solution of polyvinylferrocene (PVF) (5% PVF by weight) was dropped onto the electrode surface and dried in air. All other chemicals used were reagent grade. All solutions were made with triply distilled water. All electrochemical and EL measurements were carried out under a nitrogen atmosphere. Butyronitrile (reagent grade, Alfa Products) was purified by procedures reported previously (10a). Tetra-n-butylammonium tetrafluoroborate ($TBABF_4$) (polarographic grade, Southwestern Analytical Chemistry, Austin, Texas) was recrystallized, and tetra-n-butylammonium persulfate [$(TBA)_2S_2O_8$] was prepared as reported previously (10b).

The electrochemical cells, apparatus, and procedures of our previous study (9) were used to make all electrochemical measurements. EL spectra were obtained with a PAR Model 1215 OMA2 optical multichannel analyzer including a silicon-intensified target vidicon detector with a vacuum UV scintillator to enhance the UV response. An integrating sphere was used in the measurement of EL efficiency. Temperature variation and control was achieved with an FTS Systems (Stone Ridge, New York) Model LC-100 liquid cooler cryostat equipped with a Model TCH-1 proportional temperature controller and auxilliary heater with a heating coil immersed in a Dewar flask containing methanol. X-ray diffraction experiments were done with a General Electric SPG 2 x-ray spectrogonimeter.

Results

Single-crystal ZnS:Mn system.—Electrochemical measurements in aqueous solution.—Electrochemical measurements of Mn-doped ZnS single crystals were carried out in aqueous Na_2SO_4 solutions, both in the absence and presence of $(NH_4)_2S_2O_8$. Figure 1 shows the cyclic voltammograms (CV) for cathodic scans. Shown in Fig. 1a is the CV of a solution containing only 0.2*M* Na_2SO_4. No cathodic current appeared until the potential was scanned to about −1.5V *vs.* SCE. However, a cathodic wave starting at about −1.0V *vs.* SCE occurred when 0.2*M* $(NH_4)_2S_2O_8$ was added to the solution (Fig. 1b). At −1.8V *vs.* SCE, the current in the solution containing $(NH_4)_2S_2O_8$ was about 14 times larger than that of the solution containing only supporting electrolyte. The capacitance of a ZnS:Mn electrode in degassed aqueous solution containing 0.2*M* Na_2SO_4 (*p*H = 6) was used to obtain the Mott-Schottky plot shown in Fig. 2. The flatband potential was *ca.* −2.0V *vs.* SCE with a donor density of *ca.* 5×10^{17} cm^{-3}.

Photoluminescence.—PL spectra were measured with both bare ZnS:Mn and surface-modified ZnS:Mn crystals immersed in 0.2*M* Na_2SO_4. Figure 3a shows the PL spectrum

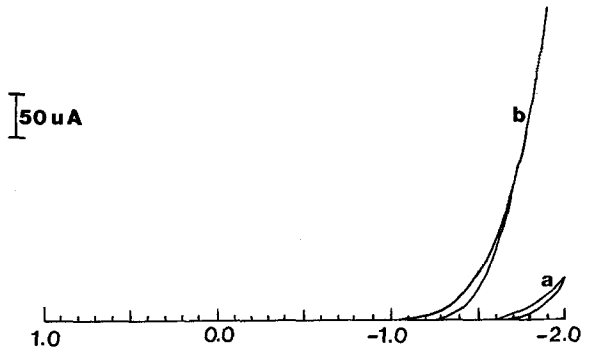

Fig. 1. Cyclic voltammogram of ZnS:Mn electrode. Scan rate, 100 mV s^{-1}. (a) 0.2M Na_2SO_4 in H_2O; (b) 0.2M Na_2SO_4, 0.2M $(NH_4)_2S_2O_8$ in H_2O.

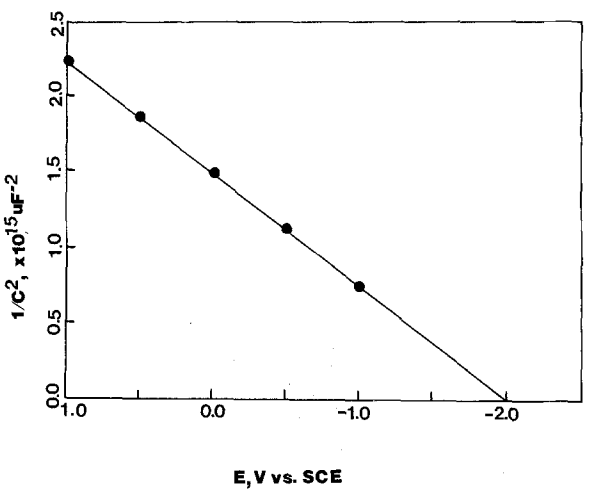

Fig. 2. Mott-Schottky plot of ZnS:Mn in 0.2M Na_2SO_4. AC frequencies, 100 and 300 Hz.

of unmodified ZnS:Mn. The emission is centered at 580 nm (excitation wavelength, 300 nm), in agreement with previous studies of this material (6). The shape of the spectrum was independent of the excitation wavelength.

The PL from ZnS electrodes is affected by applied potential (11). The PL intensity conforms to a dead-layer model, *i.e.*, the electron-hole pairs formed within a distance in the order of the depletion width do not contribute to PL (12); this permits the mapping of the electric field in

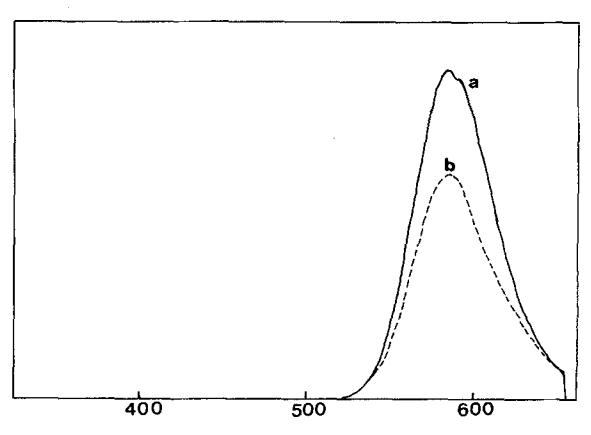

Fig. 3. Photoluminescence spectra. (a) ZnS:Mn without surface modification; (b) ZnS:Mn modified by iodine-vapor oxidized poly(vinylferrocene) film. Excitation wavelength, 300 nm.

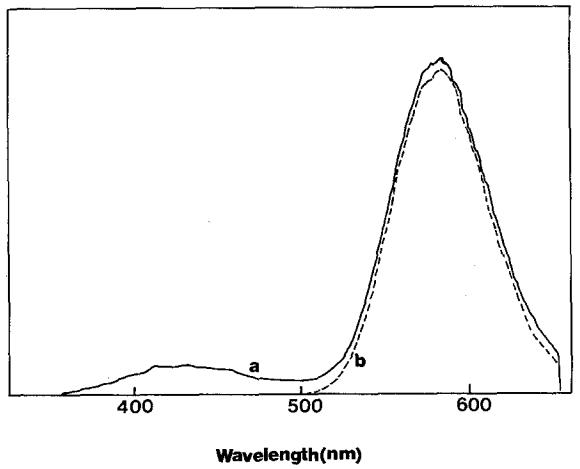

Fig. 4. Electroluminescence spectrum from ZnS:Mn. Potential pulse between 0.0 and −2.5V *vs.* SCE. Pulse width 10.0 ms. (a) Electrode with nonuniform Mn concentration distribution; (b) electrode with uniform Mn concentration distribution.

the semiconductor. Polyvinylferrocene (PVF) can be used to modify the electrode surface (13). Excitation of a PVF-modified ZnS:Mn single crystal (excitation wavelength, 300 nm) in an atmosphere of N_2 produced emission at 580 nm, identical to that of the bare ZnS:Mn crystal. When the PVF on the ZnS:Mn surface was oxidized by I_2 vapor, the PL intensity was quenched by about 20-30%, as shown in Fig. 3b (a correction was made for the absorbance of the film). The spectral distribution, however, remained unchanged.

Electroluminescence.—EL was generated by pulsing the potential of ZnS:Mn electrode in degassed aqueous solution containing $(NH_4)_2S_2O_8$. The emission could only be observed at potentials more negative than the flatband potential (V_{FB} −2.0V *vs.* SCE, as shown in Fig. 4, and as in previous studies (2), results from hole (h^+) injection into the valence band of ZnS by SO_4^- produced during $S_2O_8^{2-}$ reduction. Depending on the sample, either two peaks at 460 and 580 nm, or only one peak at 580 nm appeared. The one at 460 nm is due to the Al dopant and donor-acceptor transition (2a) and that at 580 nm to the Mn dopant. Only samples with a uniform Mn distribution, which display emission only at 580 nm, were used in further studies. The spectral distribution did not change with pulsing potential. However, as the potential became more negative, the emission intensity grew. More negative potentials also produced larger cathodic currents, suggesting that more holes were injected into the electrode leading to more intense emission. The steady-state EL intensity was proportional to the square of the current (i), as shown in Fig. 5. This suggests that the EL process is a direct consequence of e^-h^+ recombination with both e^- and h^+ generated by the cathodic current. The rise and decay of EL from single-crystal ZnS:Mn is shown in Fig. 6 for a single 1.0 ms pulse to −2.5V *vs.* SCE. The EL decay data for different pulse widths are listed in Table I. As with Al-doped ZnS (2a), there is a dead zone at the beginning of the first potential pulse where a large cathodic current was observed without generation of a significant amount of EL. But the EL decay behavior of ZnS:Mn was different from that of ZnS:Al in that at the end of potential pulse, the current fell to zero immediately, while the EL intensity persisted for some time before it too decayed to zero. The longer the potential pulse, the longer the EL intensity lasted beyond the cessation of the current. When the potential pulse widths were longer than 10.0 ms, the EL lasted about 11.0 ms longer, regardless of the potential pulse width.

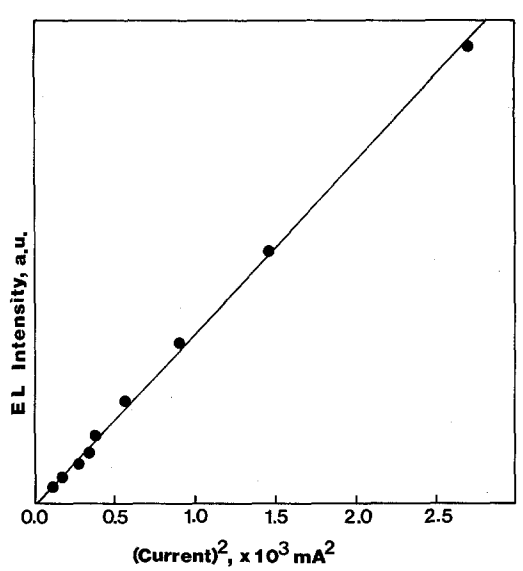

Fig. 5. Current-EL intensity relation for ZnS:Mn electrode

Effect of pH on the EL of ZnS:Mn.—EL experiments were conducted in aq. 0.2*M* $(NH_4)_2S_2O_8$ solutions as a function of *p*H. While a change in the solution *p*H did not affect the EL spectral distribution, the emission intensity varied with *p*H as shown in Fig. 7. A sharp increase in EL intensity was observed between *p*H 8 and 9, with a maximum intensity observed at *p*H = 9. The maximum EL efficieny, ϕ, photon flux/current was about 0.3% at *p*H = 9.

Effect of temperature on EL.—The effect of temperature (T) on the EL of ZnS:Mn single crystals was studied in butyronitrile solution (which has a wide available T range) containing 0.2*M* tetrabutylammonium persulfate $[(TBA)_2S_2O_8]$. The EL intensity and current as a function of potential are shown for 30° and −56°C in Fig. 8. Both the EL intensity and current responses varied with temperature, but the dependencies were different. At a given potential the current at lower temperature was much smaller than that at higher temperature. The EL intensity at low temperature was also weaker than that at higher temperature, but by a smaller factor; for example, at −4.0V *vs.* Ag, the ratio of current at 30° to that at −56°C was 14, but the ratio of EL intensity of 30°C to that at −56°C was only 2.4. Thus, the relative luminescence efficiency (ϕ) increased with a decrease in T. A plot of log (ϕ) *vs.* $1/T$ (Fig. 9) is linear with a slope of 1.6×10^3 K^{-1}, equivalent to an activation energy for excited state deactivation of 0.14 eV.

The EL spectra at different temperatures are shown in Fig. 10. The peak position of the EL spectra were essentially independent of temperature over the temperature range studied (−56°-30°C). The width at half-height [$W(T)$] increased with temperature. A plot of $W(T)$ *vs.* $T^{1/2}$ gives a straight line, as shown in Fig. 11.

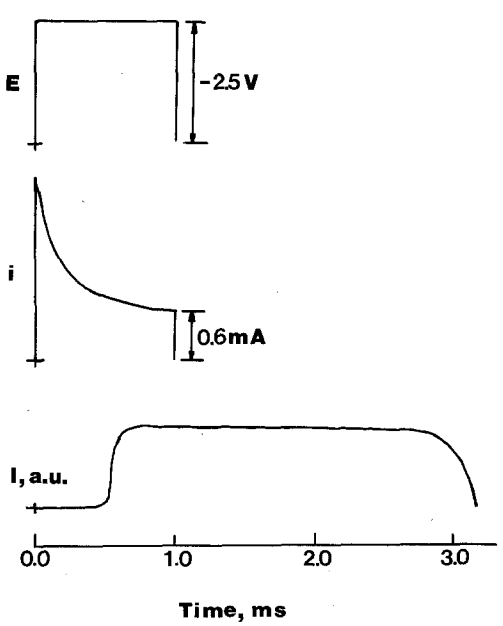

Fig. 6. Rise and decay of El from ZnS:Mn electrode for a single negative potential pulse. Potential = −2.5 *vs.* SCE. Pulse width, 1.0 ms.

Table I. Effect of pulse width on EL duration[a]

Pulse width τ(ms)	Time for EL decay to 1/2 I_o $t_{1/2}$ (ms)	Time for current decay to steady value (0.6 mA) t_o (ms)	Time delay for EL $(t_{1/2} - t_o)$ (ms)
1.0	No EL	0.0	0.0
0.2	~1.0	0.2	0.8
0.5	1.7	0.5	1.2
1.0	3.2	1.0	2.2
2.0	7.4	2.0	5.4
5.0	13.0	5.0	8.0
10.0	21.4	10.0	11.4
20.0	31.0	20.0	11.0
50.0	61.8	50.0	11.8
100.0	110.0	100.0	11.0
200.0	210.0	200.0	11.0

[a]Single-crystal ZnS:Mn electrode in aq. 0.2*M* $(NH_4)_2S_2O_8$ solution. Potential pulsed to −2.5V *vs.* SCE for τ *m*. In all cases, the steady current was 0.6 mA and the maximum EL intensity was I_o.

CVD ZnS.—Structure.—X-ray diffraction measurements show that the CVD ZnS is polycrystalline with cubic crystallites (Fig. 12). The peak at 28.5° corresponds to the (111) face, that at 47.8° to the (220) face, and that at 56.5° to the (311) face.

Electroluminescence.—For the CVD ZnS doped at different levels, the electrochemical behavior was essentially the same as that of the single-crystal Mn-doped ZnS. A Mott-Schottky plot of an Al-doped CVD ZnS electrode in degassed aqueous solution contain 0.2*M* Na_2SO_4 (*p*H ≅ 6) is shown in Fig. 13. The V_{FB} was about −2.0V *vs.* SCE with a total donor density of 2.7×10^{16} cm^{-3}. EL from the doped CVD ZnS was observed when a negative potential was applied to the electrode immersed in a solution containing 0.2*M* $(NH_4)_2S_2O_8$. The EL spectra observed for the doped CVD ZnS electrodes were characteristic of the dopant employed, as shown in Fig. 14. Al-doped CVD ZnS showed a peak at 430 nm, Cu-doped at 475 nm, and Mn-doped at 565 nm. The EL spectrum for all samples was unaffected by a change in the applied potential. The integrated EL efficiencies of these doped CVD ZnS electrodes were of the order of 0.2%.

Discussion

Photoluminescence.—Manganese(II) is a well-known activator in many crystals (5). As an activator in ZnS phosphors, manganese gives a characteristic yellow-orange emission. The photoluminescence (Fig. 3) gives a peak at wavelength 580 nm in accordance with previously reported solid-state EL results (6). The crystal field approach (5) may be used for describing an isolated Mn luminescence center in ZnS. The energy-level system for the free manganese ion, Mn^{2+} ($3d^5$) gives the spherically symmetrical ^6S state as the ground state, in which all 3d electron spins are parallel. The first excited state is ^4G, where two electrons are spin-paired. The series of levels for the ion is as follows

$$^6S, {}^4G, {}^4P, {}^4D, {}^4F$$

Under a cubic crystal field, ^6S remains $^6A_1$ and ^4G splits into $^4T_1$, $^4T_2$, $^4A_1$, and ^4E. The yellow-orange emission has been assigned to the $^4T_1(^4G)$-$^6A_1(^6S)$ transition. Although this is a spin-forbidden transition, the selection rule is relaxed in crystals by crystal field perturbation, phonon coupling, and spin-orbit interaction.

The state of the crystal surface has an important effect on the PL intensity of ZnS:Mn (11). The dependence of the surface potential on PL intensity has been reported for n-type BaAs and CdS using a Schottky barrier to control the surface potential (14) and for n-InP using both Schottky barrier and oxygen absorption control (15). More recently, the PL response of palladium-cadmium sulfide and palladium-graded cadmium sulfoselenide Schottky diodes to molecular hydrogen (16) and photoluminescent properties of a derivatized GaAs surface undergoing redox chemistry have been reported (17). In each case, the PL intensity conforms to a dead-layer model that permits the

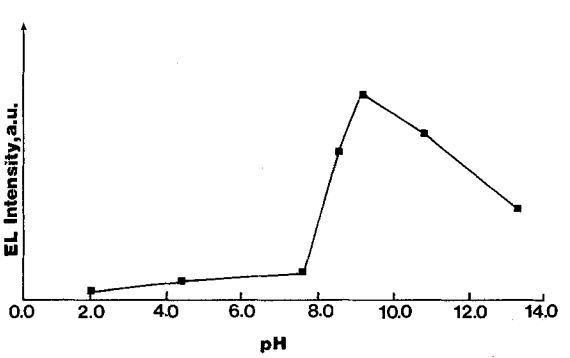

Fig. 7. *p*H-EL intensity relation for ZnS:Mn electrode. Potential pulse between 0.0 and −2.5V *vs.* SCE. Pulse width, 10.0 ms.

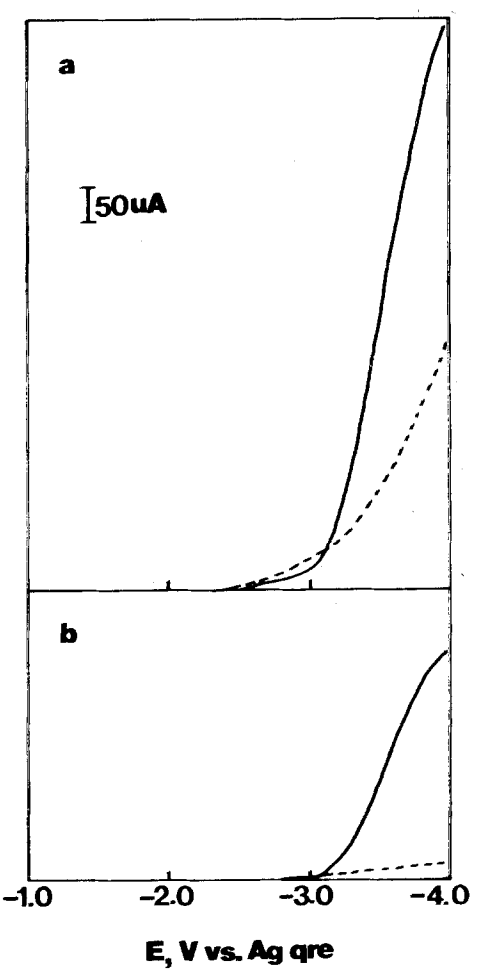

Fig. 8. Effect of temperature on EL efficiency of ZnS:Mn electrode: (a) At 30°C, (b) −56°C. _____ EL intensity; ------- current. (a) and (b) are in the same scales.

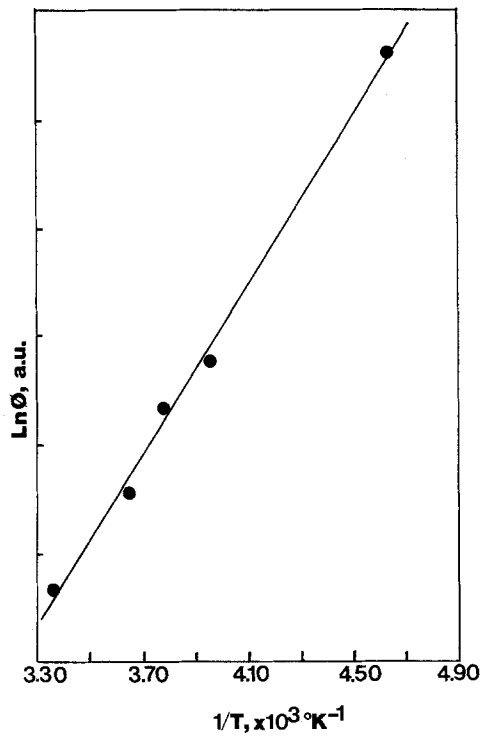

Fig. 9. Ln ϕ + 1/T plot for ZnS:Mn electrode

mapping of the electric field in the semiconductor. In this model, electron-hole pairs formed within a distance of the order of the depletion layer width do not contribute to PL (12, 16, 17). When excitation radiation entering the semiconductor is absorbed exponentially with an absorption coefficient, α, (with neglect of absorption of the sub-bandgap energy emission), the PL intensity, dI_{PL}, between x and $x + dx$ form the semiconductor surface given by

$$dI_{PL} = \phi_{PL} I_o e^{-\alpha x} dx \quad [1]$$

in which I_o is the incident excitation intensity and ϕ_{PL} is the PL quantum efficiency. If ϕ_{PL} is independent of x in the bulk and the intensity of the radiative recombination in the space-charge region is significantly lower than that in the bulk, one can obtain the integrated PL intensity, I_{PL}, given in Eq. [2]

$$I_{PL} = I_{PL}^{FB} \exp(-\alpha D) \quad [2]$$

in which I_{PL}^{FB} is the integrated PL intensity at the flatband potential, V_{FB}, (*i.e.*, when $D = 0$), where D is the width of the depletion layer.

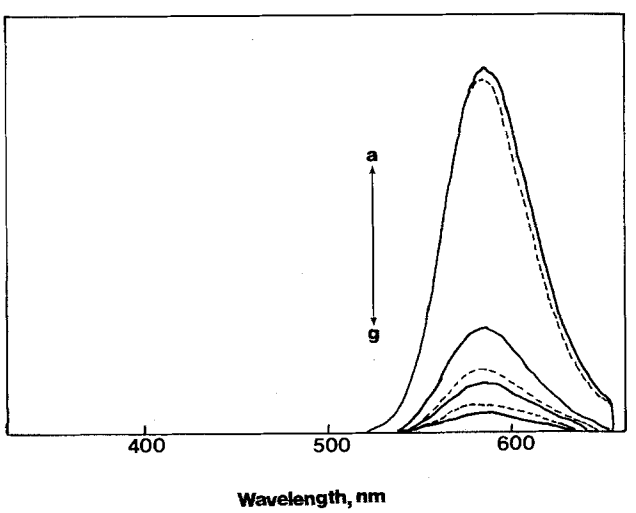

Fig. 10. EL spectra of ZnS:Mn electrode at different temperatures. Potential pulse between 0.0 and −4.0 *vs.* Ag. Pulse width, 10.0 ms. (a) 24°C, (b) 10°C, (c) −2°C, (d) −10°C, (e) −20°C, (f) −31°C, and (g) −40°C.

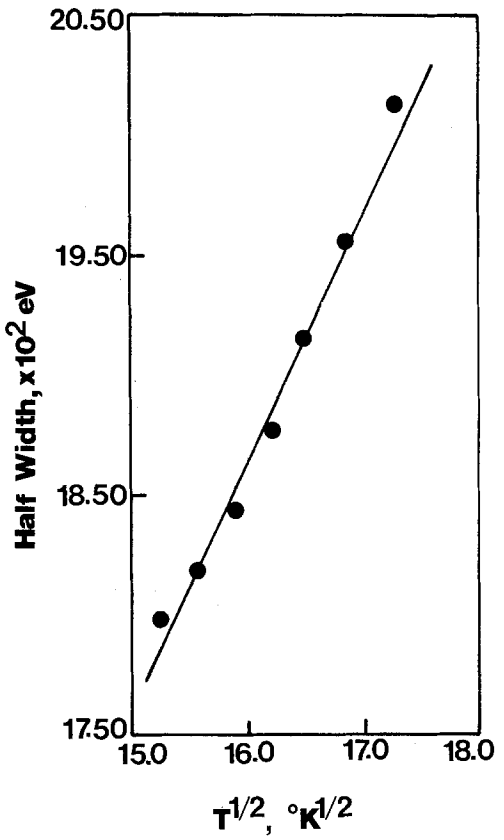

Fig. 11. The dependence of the square root of temperature ($T^{1/2}$) on the half-height width of spectra [$W(T)$].

Equation [2] corresponds to a simplified form of Eq. [3] derived previously (14b), with the assumptions $SL_h/D_h >> 1$ and $[Se^{-\alpha D}L_h/D_h(1 + \alpha L_h)] >> 1$, where S is the effective surface recombination rate, L_h and D_h are, respectively, the diffusion length and the diffusion coefficient of holes

$$I_{PL} = [\phi_{PL} I_s/(1 + SL_h/D_h)][1 + (e^{-\alpha D}/1 + \alpha L_h) SL_h/D_h] \quad [3]$$

where I_s is the exciting light intensity. The implication of Eq. [2] and [3] under those assumptions is that I_{PL}^{FB} is given by $\phi_{PL} I_s/(1 + \alpha L_h)$.

The change of the PL intensity of ZnS:Mn induced by the I_2-oxidized PVF film might be indicative of two effects: the change in the width of the space-charge layer and the change in the surface recombination rate of ZnS:Mn. The PL intensity, as expected, decreases with increasing dead-layer thickness when the coated PVF film is oxidized. Assuming that the ZnS:Mn surface recombination rate is very large, we can estimate the change in the dead-layer thickness, ΔD, to be *ca.* 260Å at 300 nm by taking $\alpha = 1.2 \times 10^5$ cm^{-1} (18).

Electroluminescence.—The EL spectrum of ZnS:Mn electrodes (Fig. 4) has a peak at 580 nm. The fact that the EL and PL spectra are the same indicates the same luminescence center is involved. The mechanism of EL from a semiconductor/electrolyte interface with $S_2O_8^{2-}$ is probably the same as in previous studies (1-2). When the semi-

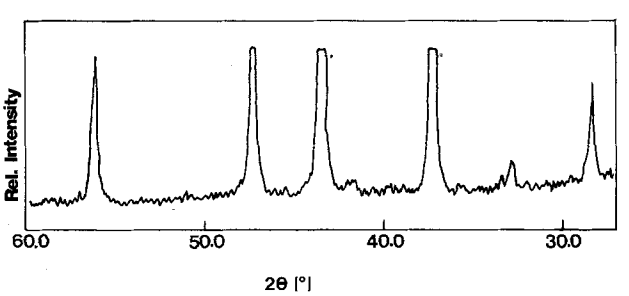

Fig. 12. X-ray diffraction spectra of CVD ZnS. Peaks marked with * are due to Al substrate.

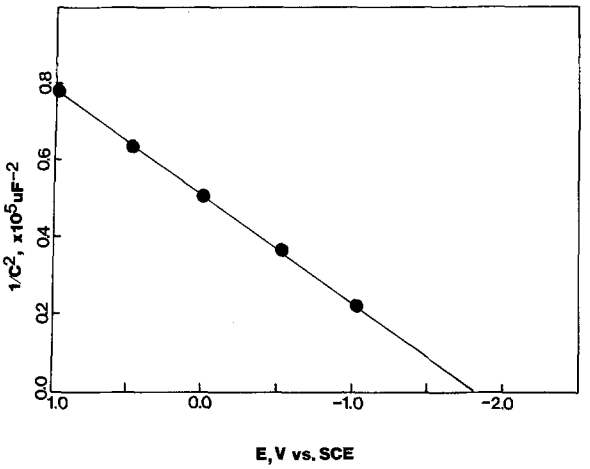

Fig. 13. Mott-Schottky plot of Al-doped CVD ZnS in 0.2M Na_2SO_4. AC frequencies, 100 and 300 Hz, pH 9.

conductor electrode is negatively biased, the anion $S_2O_8^{2-}$ is reduced by conduction band (cb) electrons to generate strongly oxidizing SO_4^{-}, which injects holes into the valence band (vb). The vb holes then undergo various radiative and nonradiative recombination processes with electrons through recombination centers. The mechanism of EL for ZnS:Mn is shown in Eq. [4]-[8]

$$S_2O_8^{2-} + e^- (cb) \rightarrow SO_4^{2-} + SO_4^{-} \quad [4]$$

$$SO_4^{-} \rightarrow SO_4^{2-} + h^+ (vb) \quad [5]$$

$$Mn^{2+} + h^+(vb) \rightarrow Mn^{3+} \quad [6]$$

$$Mn^{3-} + e^-(cb) \rightarrow Mn^{2+} \quad [7]$$

$$Mn^{2+*} \rightarrow Mn^{2+} + hv \quad [8]$$

Mn^{2+} could also trap a cb electron, which could recombine with h^+ or Mn^{3+} to generate Mn^{2+*}. The present experimental results cannot differentiate between these alternative routes. However, the intensity-current relation does suggest a double injection mechanism for the luminescence process, since the intensity is proportional to the square of the current (2a).

At bias potentials negative of V_{FB}, the depletion layer width diminishes and holes generated in process (5) can easily diffuse away from the (ZnS/solution) interface into the bulk of the semiconductor where they are captured by Mn^{2+} to produce Mn^{3+}, which might be the precursor of Mn^{2+*}. The concentration profile of Mn^{3+} is apparently dependent on the rate of process (6), the diffusion coefficient of holes, D_h, and the lifetime, τ, of Mn^{2+*}. Since τ is fairly long (*ca.* 1.77 ms) (19) and D_h is large (*ca.* 0.39 cm^2s^{-1}) (20),

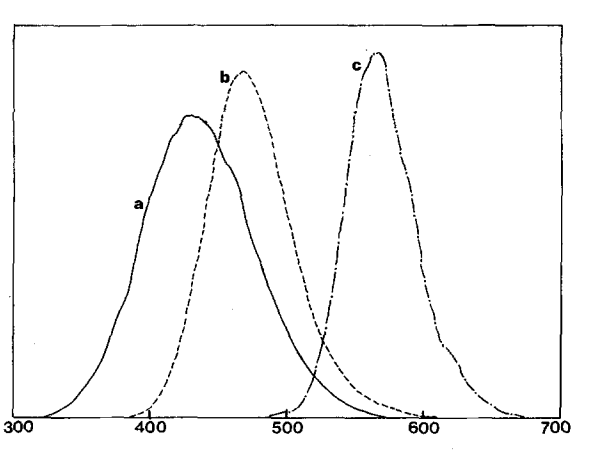

Fig. 14. EL spectra of CVD ZnS. Potential pulse between 0.0 and −3.0V vs. SCE, pulse width, 10 ms. (a) Al-doped, (b) Cu-doped, and (c) Mn-doped.

Mn^{3+} can be deeply distributed inside the bulk (a few hundred μm from the surface) when large numbers of holes are injected and no Mn^{3+} is consumed by other processes. Once the electrode is reverse-biased, these trapped holes (*i.e.*, Mn^{3+}) could be responsible for the slow decay of the EL, because electrons are now depleted from the surface layer, slowing down the process (7). Note that a very short negative potential pulse can only generate Mn^{3+} near the surface, where nonradiative recombination could be very fast as assumed in the previous section. In this case the EL decay would be fast. Those arguments, based on the spatial distribution, diffusion and trapping of charge carriers, or excited states, are qualitatively consistent with the results shown in Table I and Fig. 6.

The effect of pH on the EL of ZnS:Mn.—Plots of zeta potential of ZnS in aqueous solution as a function of pH show three distinct regions (21). There is a plateau between pH 4 and 8.5 where the zeta potential (which is the measure of the potential difference across the double layer) has a nearly constant negative value. At pH > 8.5, the zeta potential remains negative but increases in magnitude. At pH < 3, the zeta potential becomes positive. Dissolution of surface layers by acid-base reactions can occur at both low (<3) and at high (>9) pH. The decrease of EL intensity in these two regions (Fig. 7) might be caused by these surface reactions. Another factor that decreases the EL intensity at pH < 5 involves the competition between the reduction of protons and $S_2O_8^{2-}$ on the ZnS:Mn electrode. For the pH region between 5 and 9, variation of EL intensity might be explained by the change of the interfacial energetics upon the variation of pH. The pH shifts V_{FB} according to Eq. [9]

$$qV_{FB} = \text{Const.} + 2.3\,kT\,(pzzp\text{-}pH) \quad [9]$$

where *pzzp* is the point of zero zeta potential. A higher pH produces a more negative V_{FB} (2a) favoring hole injection into the valence band which should result in an increase in EL intensity. This is consistent with the results obtained between pH 5 and 9.

Effect of temperature on EL.—High temperatures decrease the EL efficiency (Fig. 9). The quenching of the usual yellow radiation from a transition within the $3d^5$ shell of manganese in low-resistivity ZnS appears to be an Auger process (22). In the Auger process, an impurity in an excited state loses its energy to a charge carrier. In our EL experiments, fairly conductive ZnS samples (with donor density *ca.* 10^{18} cm^{-3}) were used, and EL was observed at potentials negative of V_{FB}. Those conditions are favorable for Auger processes to take place. By assuming that the quenching rate is linearly proportional to the carrier concentration, N, and N varies with temperature as $N_o \exp(-E/kT)$, one obtains (22)

$$(1 - \phi)/(\phi = C \exp(-E/kT) \quad [10]$$

where ϕ is the efficiency, C is a constant involving radiative and nonradiative lifetimes (both assumed to be independent of temperature), k is Boltzmann's constant, and T is temperature. E is the thermal ionization energy of shallow donors. When ϕ is much smaller than unity, the expression becomes

$$1/\phi = C \exp(-E/kT) \quad [11]$$

$$\ln \phi = -\ln(C) + (E/kT) \quad [12]$$

A plot of $\ln \phi$ *vs.* $1/T$ (Fig. 9) yields a straight line with a slope of E/k. From the slope, E = 0.14 eV, in reasonable agreement with the value of 0.17 eV obtained previously (22).

The emission curve of ZnS:Mn can be understood by a configuration diagram scheme (23). In the simplest treatment utilizing this model, the approximation is made that only one localized vibrational mode interacts strongly with the luminescence center. The observed emission band is considered to be an envelope containing numerous lines, each of these lines due to a transition between one vibrational level, n, of the excited electronic state and one vibrational level, m, of the ground electronic state. The spectral distribution of emission is given by Eq. [13]

$$I(h\nu) = 64\pi^4\nu^4/3c^3 \sum_m \sum_n \exp(-nh\nu_e/kT) |\mathrm{Meg}^{nm}|^2 \delta(E_e^h - E_g^m - h\nu) \quad [13]$$

with use of Franck-Condon approximation, where Meg^{nm} is the matrix element for the electric dipole transition. One of the important results of the configuration coordinate model is the form of the temperature dependence of the emission band width at half-maximum $W(T)$

$$W(T) = W(0)[\coth(h\nu_e/2kT)]^{1/2} \quad [14]$$

where $W(0)$ is the width at $T = 0$ K, and ν_e is the frequency of the vibrational mode that interacts strongly with the luminescence center in its excited electronic state. At high temperature ($2kT >> h\nu_e$), $W(T)$ varies as $T^{1/2}$. The present experimental results obey this relationship (Fig. 11).

CVD ZnS.—Differently doped CVD ZnS electrodes produce EL via different mechanisms. Donor-acceptor pairs are usually responsible for the blue emission from Al-doped ZnS crystals (2). For a Cu-doped ZnS crystal where copper acts as an activator, the emission is due to the electronic transition from conduction band to Cu center (5). Mn-doped ZnS crystals give the characteristic emission of Mn^{2+}. The typical emission spectra have maxima at 460, 520, and 580 nm for Al-, Cu- and Mn-doped single-crystal ZnS, respectively. The emission maxima for the corresponding CVD polycrystalline ZnS are blue-shifted from those values and appear at 430, 475, and 565 nm, respectively (see Fig. 14). This may be due to the differences in the crystal forms. The doped CVD polycrystalline ZnS has a high EL efficiency, comparable to that of single-crystal ZnS (2). This suggests that CVD ZnS is a good candidate for EL studies.

Acknowledgment

The support of this research by the Army Research Office and the National Science Foundation (CHE8304666) is gratefully acknowledged. We are indebted to Professor J. McCaldin for the single-crystal ZnS samples.

Manuscript submitted March 1, 1988; revised manuscript submitted Aug. 8, 1988.

The University of Texas assisted in meeting the publication costs of this article.

REFERENCES

1. (a) H. H. Strickert, J.-R. Tong, and A. B. Ellis, *J. Am. Chem. Soc.*, **104,** 581 (1982); (b) B. R. Karas, H. H. Strickert, R. Schreiner, and A. B. Ellis, *ibid.*, **103,** 1648 (1981).
2. (a) F.-R. F. Fan, P. Leempoel, and A. J. Bard, *This Journal,* **130,** 1866 (1983); (b) F.-R. F. Fan and A. J. Bard, *J. Phys. Chem.*, **89,** 1232 (1985).
3. M. Aven and J. S. Prener, "Physics and Chemistry of II-VI Compounds," John Wiley and Sons, New York (1967).
4. D. Theis, *J. Lumin.*, **23,** 191 (1981).
5. D. Curie, "Luminescence in Crystals," Methuen, London (1963).
6. P. Goldberg, "Luminescence of Inorganic Solids," Academic Press, New York (1966).
7. A. B. Ellis in "Chemistry and Structure at Interfaces: New Laser and Optical Techniques," R. B. Hall and A. B. Ellis, Editors, Chap. 6, VCH Publishers, Deerfield Beach, Florida (1986).
8. R. G. Kaufman and P. Dowbor, *J. Appl. Phys.*, **45,** 4487 (1974).
9. F.-R. Fan, H. S. White, B. L. Wheeler, and A. J. Bard, *J. Am. Chem. Soc.*, **102,** 5412 (1980).
10. (a) R. P. Duyne and C. N. Reilley, *Anal. Chem.*, **44,** 142 (1972); (b) W. G. Becker, H. S. Seung and A. J. Bard, *J. Electroanal. Chem.*, **127,** 167 (1984).
11. I. K. Vershchagin and E. A. Serov, *Zh. Prikl. Spektr.*, **35,** 450 (1981).
12. R. E. Hollingsworth and J. R. Sites, *J. Appl. Phys.*, **53,** 5357 (1982).
13. A. Merz and A. J. Bard, *J. Am. Chem. Soc.*, **100,** 3222 (1978).
14. (a) V. Langmann, *Appl. Phys.*, **1,** 219 (1973); (b) G. K. Volodina, L. I. Gorshkov, G. P. Peka, and V. I. Strikha, *J. Appl. Spect.*, **29,** 1077 (1978); (c) R. E. Hetrick and K. F. Yeung, *J. Appl. Phys.*, **42,** 2882 (1971).
15. (a) K. Ando, A. Yamamoto, and M. Yamaguchi, *J. Appl. Phys.*, **51,** 6432 (1980); (b) K. Ando, A. Yamamoto, and M. Yamaguchi, *Jpn. J. Appl. Phys.*, **20,** 1107 (1981); (c) R. A. Street, R. H. Williams, and R. S. Bauer, *J. Vac. Sci. Technol.*, **17,** 1001 (1980).
16. M. K. Carpenter, H. Van Ryswyk, and A. B. Ellis, *Langmuir*, **1,** 605 (1985).
17. H. Van Ryswyk and A. B. Ellis, *J. Am. Chem. Soc.*, **108,** 2454 (1986).
18. E. Khawaja and S. G. Tomlin, *J. Phys. D: Appl. Phys.*, **8,** 581 (1975).
19. H.-E. Gumlich, *J. Lum.*, **23,** 73 (1981).
20. Y. V. Voronov, in "Radiative Recombination in Semiconductor Crystals," D. V. Skobel'tsyn, Editor, Proceedings of the Lebedev Physical Institute, p. 1 (1986).
21. R. Williams and M. E. Labib, *J. Colloid Interface Sci.*, **106,** 251 (1985).
22. N. T. Gordon and J. W. Allen, *Solid State Commun.*, **37,** 441 (1981).
23. M. Balkanski, R. Beserman, and D. Langer, in *Proc. Int. Conf. Lum.*, 1186-1190 (1966).